Full Paper

Journal of the Brazilian Chemical Society

https://dx.doi.org/10.21577/0103-5053.20250103

J. Braz. Chem. Soc. **2025**, *36*, 10, e-20250103, 1-15

In vivo and *in silico* Evaluation of Cashew Nut Shell Liquid and Ag-CNSL Nanoparticles for Anxiolytic Activity in Zebrafish via GABAergic Pathways

Thayllan T. Bezerra,[a] Mayara O. Almeida,[a] Pergentino N. Maia Júnior,[b] Emerson Y. A. Sousa,[a] Maria K. A. Ferreira,[b] Antonio W. Silva,[b] Giuseppe Mele,[c] Emmanuel S. Marinho,[d] Hélcio S. Santos,[b,e] Jane E. S. A. Menezes,[b] Diego Lomonaco[a] and Selma E. Mazzetto[a]

[a]*Departamento de Química Orgânica e Inorgânica, Universidade Federal do Ceará, 60020-181 Fortaleza-CE, Brazil*

[b]*Centro de Ciência e Tecnologia, Universidade Estadual do Ceará, 60741-000 Fortaleza-CE, Brazil*

[c]*Department of Engineering for Innovation, University of Salento, via Arnesano, 73100 Lecce, Italy*

[d]*Departamento de Química, Universidade Estadual do Ceará, 62930-000 Limoeiro do Norte-CE, Brazil*

[e]*Curso de Química, Universidade Estadual do Vale do Acaraú, 62010-295 Sobral-CE, Brazil*

This paper presents the anxiolytic potential of the major constituents of cashew nut shell liquid (CNSL), anacardic acid (AA), cardanol (CDN), and cardol (CD), and CNSL-derived silver nanoparticles (AgAA and AgCD) compared to diazepam (DZP) in zebrafish (*Danio rerio*) and *in silico* by docking on the GABAergic system. CD and CDN were extracted and purified using silica gel column chromatography, and AA was extracted by acid-base reaction. Silver nanoparticles were synthesized through microwave-assisted reduction of silver nitrate with CNSL constituents. UV-Vis spectroscopy presented surface plasmon resonance extinction peaks at 423 (AgAA) and 414 nm (AgCD). Transmission electron microscopy revealed spherical nanoparticles within liposomes of AA and CD. All tested drugs had no toxicity below 40 ppm. CDN (40 ppm) decreased locomotion by 76.98%, approaching DZP (90.67%). AA, CDN, CD, and AgAA surpassed the anxiolytic effect of DZP in the light/dark test, while AgCD was ineffective. Flumazenil reversed the anxiolytic effect of all compounds, confirming GABAergic mediation. Molecular docking revealed that di-unsaturated CD had the highest $GABA_A$ affinity, and di-unsaturated AA mimics the hydrophobic profile of DZP. Results confirmed the anxiolytic potential of CNSL, and the synthesis of CNSL-capped AgNPs gives water-soluble anxiolytic drugs with a controlled-release mechanism.

Keywords: CNSL, AgNPs, anxiolytic effect, zebrafish, docking, $GABA_A$

Introduction

According to the World Health Organization (WHO), anxiety and depression are the most common mental disorders, affecting more than 301 million people worldwide, especially women and the elderly.[1] The International Classification of Diseases (ICD-11) considers anxiety disorders of the central nervous system (CNS) as apprehensiveness or anticipation of future danger or misfortune accompanied by a feeling of worry, distress, or somatic symptoms of tension, like excessive worry or fear of a specific situation, resulting in restlessness, fatigue, lack of concentration, irritability, and insomnia. Meanwhile, depressive disorders are characterized by low mood or loss of pleasure and interest in activities, for long periods accompanied by other cognitive, behavioral, or neurovegetative symptoms that significantly affect the individual's ability to function.[2-7]

Benzodiazepines (BZD) are a class of drugs administered to treat anxiety, insomnia, and seizures since the 1960s.[5,6] BZDs act on the central nervous system as positive allosteric modulators of the gamma-aminobutyric acid ($GABA_A$) receptor, a ligand-dependent, chloride-selective ion channel.[7,8] Human $GABA_A$ receptors consist of 19 identified subunits: α_{1-6}, β_{1-3}, γ_{1-3}, δ, ε, θ, π, and ρ_{1-3}, which form a restricted set of receptor subtypes. Predominantly, the $GABA_A$ receptors in the brain are

*e-mail: thayllanteixeirabezerra@gmail.com
Editor handled this article: Hector Henrique F. Koolen (Associate)

heteropentamers composed of two α, two β, and one γ or δ subunit.[9,10] Diazepam (DZP, $C_{16}H_{13}ClN_2O$), a non-selective BZD, interacts with the α_1 subunit, causing sedative and anesthetic effects. Anxiolytic and myorelaxant effects come from the interaction of BZD with α_2 and α_3 subunits, while the anticonvulsant effect is mediated through the α_1, α_2, and α_5 subunits.[10,11]

The Diagnostic and Statistical Manual of Mental Disorders (DSM-5) establishes criteria for substance abuse, like escalating dosage, developing tolerance and cravings for the drug effects, and the loss of self-control.[12] The increase in tolerance and abuse of benzodiazepines (BZDs) comes from attempts to manage emotional and/or physical distress, such as anxiety, depression, and insomnia, consistent with their therapeutic indications, however, in patients with chronic abuse of BZDs, the brain relies on the drug to maintain normal functioning, thereby increasing the number of GABA receptors and increasing the risk of dependence and substance abuse.[11,13] BZDs have been associated with the likelihood of developing neurocognitive impairments and Alzheimer's disease.[11,14] The limitations of BZDs require alternative treatments, such as plant-based medicines, which have shown efficacy in treating anxiety disorders.[15]

Among natural products, the cashew nut shell liquid (CNSL) is a promising candidate. CNSL is a dark, viscous liquid obtained from the shell of the cashew nut (*Anacardium occidentale* L.). It comprises four phenolic lipids (Figure 1) with a 15-carbon alkyl side chain: anacardic acid (AA), cardol (CD), cardanol (CDN), and 2-methylcardol (2-MCD). Each CNSL constituent is obtained as a mixture of saturated, mono, di, and tri-unsaturated homologs. AA (65%) is the main component of natural CNSL, however, the industrial processing roasts the cashew nut at 190 °C, causing decarboxylation of AA, resulting in CDN as the primary component of what is now called technical CNSL.[16-20]

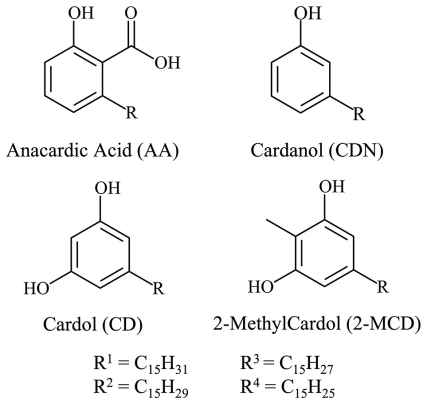

Figure 1. Chemical structure of CNSL constituents, where R represents a 15-carbon alkyl chain that can be saturated ($R^1 = C_{15}H_{31}$), mono ($R^2 = C_{15}H_{29}$), di ($R^3 = C_{15}H_{27}$) or tri-unsaturated ($R^4 = C_{15}H_{25}$).

CNSL exhibits a range of important pharmacological activities, acting as antimicrobial,[21] ovicidal, larvicidal, and pupicidal,[22] acetylcholinesterase inhibitor,[23] dengue virus inhibitor,[24] and leishmanicidal.[25] The anacardic acids from CNSL have shown $GABA_A$-mediated anxiolytic effects without myorelaxant or genotoxic effects.[26,27]

CNSL can enhance pharmacological features by assembling noble metal nanoparticles. Silver nanoparticles (AgNPs) have tunable chemical and physical properties, making them versatile tools in biomedicine[28] as prime candidates for drug delivery systems, reducing the toxicity of organic compounds.[29]

Animal models, such as adult zebrafish (*Danio rerio*), are commonly used to investigate the effects of novel compounds in various human brain disorders, e.g., depression and anxiety.[30-33] Zebrafish are suitable for evaluating new anxiolytic drugs due to their conserved neurotransmitters that share more than 80% of orthologous genes related to human diseases.[15,34]

Based on the above, this study evaluated the toxicity and anxiolytic effects of CNSL major constituents and CNSL-capped AgNPs in an *in vivo* model with adult zebrafish (*Danio rerio*), and *in silico* with molecular docking to analyze the binding affinity energy and interaction type with $GABA_A$ receptors.

Experimental

Drugs and reagents

Amêndoas do Brasil (Fortaleza, Brazil) supplied natural and technical CNSL. The reagents and drugs used were ethyl acetate ($C_4H_8O_2$, Vetec Química, purity ≥ 99%) and *n*-hexane (C_6H_{14}, Vetec Química, purity ≥ 99%), diazepam (DZP, $C_{16}H_{13}ClN_2O$, CAS 439-14-5, Neo Química; EAN: 7896714232980), flumazenil (FMZ, $C_{15}H_{14}FN_3O_3$, CAS 78755-81-4, Sandoz, DIN: 02249561), and dimethyl sulfoxide (DMSO, $(CH_3)_2SO$, Dinâmica, purity ≥ 99%).

Instrumentation

The ^1H and ^{13}C nuclear magnetic resonance (NMR) spectra of AA, CDN, and CD were recorded on a Bruker Avance DPX 300 spectrometer. For ^1H NMR, the equipment operated at 300 MHz with a zg30 pulse program (16 scans, 1 s relaxation delay, 32,000 data points; spectral width: 20 ppm). For ^{13}C NMR, the equipment operated at 75 MHz with zgpg30 pulse program (1024 scans, 2 s relaxation delay, 64,000 data points; spectral width: 240 ppm). The samples (10 mg mL^{-1}) were dissolved in deuterated chloroform ($CDCl_3$) at 25 °C, with the solvent serving as the

internal reference (peaks at 7.26 ppm for ^{1}H, 77.16 ppm for ^{13}C). The gas chromatography-mass spectrometry (GC-MS) analyses of CDN and CD were performed in a Shimadzu GC-MS-QP 2010 chromatograph with electron impact ionization at 70 eV (*m/z* 50-500, ion source at 200 °C and interface at 280 °C), equipped with a DB-5 column (5%-phenyl)-methylpolysiloxane, measuring 20-m length with 0.18-mm internal diameter, and 0.4-µm film thickness. The column temperature program started at 50 °C for 2 min, and increased to 280 °C at 10 °C min^{-1}, held for 5 min. A 1 µL of each sample was injected. Helium was used as the carrier gas at a flow rate of 1.0 mL min^{-1}, with the injector temperature at 250 °C. The ultraviolet-visible (UV-Vis) spectra of AgAA and AgCD (0.1 mg mL^{-1}, based on CNSL content) were recorded on an Agilent Cary 60 spectrophotometer. Samples were scanned from 200-800 nm at a 10 nm s^{-1} rate in a 1-cm quartz cuvette. The infrared (IR) spectra of AA, CDN, and CD were recorded on a PerkinElmer Frontier FTIR/NIR (Fourier-transform infrared/near infrared) spectrophotometer coupled with the attenuated total reflectance (ATR) technique. The resolution was set at 4 cm^{-1} with four scans from 4000-550 cm^{-1}. The morphology of AgAA and AgCD was established by transmission electron microscopy (TEM) in a Jeol JEM 1011 operating at 100 kV equipped with a camera Gatan Orius model 831. Each sample was deposited onto a copper grid and dried inside an oven at 60 °C overnight prior to the analysis. The dynamic light scattering (DLS) analysis of AgAA and AgCD was performed using a Malvern Zetasizer ZS90 (Malvern Panalytical) at a 90° scattering angle (633 nm laser) in deionized water (viscosity: 0.8872 cP, refractive index: 1.33) at 25 ± 0.1 °C with 120 s equilibration. The samples were freshly prepared before analysis, and the detection range of the instrument was set at 0.3 nm-5 µm. Three independent measurements of 20 runs were conducted, and the particle size distributions were calculated using the cumulants method.

Isolation and purification of CNSL constituents

Cardol (CD) and cardanol (CDN) were isolated from 30 g of technical CNSL using a modified method.[35] The constituents were separated using column chromatography on silica gel with a stepwise gradient of *n*-hexane: ethyl acetate (9:1 to 7:3 v/v), eluting in order: CDN, 2-MCD, and CD. Thin-layer chromatography was used to analyze the collected fractions, which were then concentrated through rotary evaporation under reduced pressure. The solvent was condensed and further purified. The isolation yielded 20.0 ± 0.84 g (66.7 ± 2.8%) of CDN and 4.75 ± 0.36 g (15.8 ± 1.2%) of CD based on three independent isolations of 30 g of CNSL. Both compounds were characterized by GC-MS, ^{1}H NMR and ^{13}C NMR, and FTIR-ATR (Figures S1-S8, Supplementary Information (SI) section).

Anacardic acid (AA) was isolated from 10 g of natural CNSL using a modified method.[36] Natural CNSL (10 g) was diluted with 100 mL of 90% (v/v) methanol:water solution in a 250 mL reaction flask fitted with a condenser. Calcium hydroxide (5 g) was poured into the flask and stirred vigorously at 50 °C for 90 min, resulting in a rose-colored precipitate, calcium anacardate (CaAA). The solid was filtered and washed ten times with 10 mL of methanol to remove residues of other CNSL constituents. CaAA was dried at 60 °C for 2 h, then transferred to a separatory funnel with 50 mL of 5% hydrochloric acid (HCl) and shaken vigorously for 5 min. The protonation converted CaAA to AA. Ethyl acetate (50 mL) was added to the separatory funnel to extract AA into the organic phase. The aqueous phase was discarded. The organic phase was washed three times with brine to remove HCl and water-soluble residues. The AA solution was dried with anhydrous sodium sulfate (Na_2SO_4), and the solvent was rotary evaporated under reduced pressure at 40 °C, yielding 6.25 ± 0.32 g of AA (62.5 ± 3.2%; n = 3 independent isolations). AA was characterized using ^{1}H NMR and ^{13}C NMR, and FTIR-ATR (Figures S9-S11, SI section).

Synthesis of silver nanoparticles

AA (13.8 mg, 40 µmol) and CD (12.7 mg, 40 µmol) were solubilized in an aqueous solution of sodium hydroxide (NaOH, 1.25 mmol L^{-1}, 8 mL). CDN has the lowest solubility in water among all constituents, even in basic conditions, thus, it was excluded from the experiment.

Silver nitrate ($AgNO_3$, 1.7 mg, 10 µmol, 1 mL) was added to AA and CD solutions, respectively. The mixture was transferred to a two-neck flask coupled to a condenser in a microwave reactor and heated to 60 °C (400 W) and stirred for 2 min. Then, sodium borohydride ($NaBH_4$, 3.8 mg, 10 µmol, 1 mL, freshly prepared), was added dropwise over 30 s at a rate of 2 mL min^{-1} to reduce the silver ions (Ag^+:$NaBH_4$; molar ratio of 1:1), and stirring was maintained at 200 rpm (rotations *per* min) throughout the experiment. Upon contact with $NaBH_4$, the solution turned yellow. Heating and stirring were maintained for an additional 5 min to ensure a complete reduction of the silver ions. AgAA and AgCD were stored in a flask protected from light to prevent oxidation. AgAA and AgCD were characterized by UV-Vis spectroscopy, size (Figures S12 and S14 (SI section), respectively), and morphology was determined by TEM. DLS was used to determine the hydrodynamic size (Figures S13 and S15, SI section) and polydispersity index (PDI).

Adult zebrafish (*Danio rerio*)

Adult zebrafish (396 fish; age 60-90 days, 0.4 ± 0.1 g, 3.5 ± 0.5 cm) were randomly selected from a mixed population obtained from Bio Pet Comércio de Produtos Veterinários LTDA (Fortaleza, Brazil). Each experimental group (n = 6) had an even number of males and females (3 males and 3 females) to minimize sex-related variability in behavioral and pharmacological responses,[37] and to ensure randomization as *per* the ARRIVE (animal research: reporting of *in vivo* experiments) guidelines.[38] This method warrants representativeness and maintains the sample size, aligning with previous studies of anxiolytic drugs in zebrafish.[39]

Zebrafish (n = 3 *per* liter) were placed in a 10-L glass aquarium (30 cm × 15 cm × 20 cm) filled with dechlorinated water (25 ± 1 °C and the pH at 7.0), treated with Protectplus (chlorine neutralizer), and equipped with submerged filters and air pumps. Fish were kept in a 14-h/10-h light/dark cycle and fed with spirulina *ad libitum* for 7 days. Feeding was suspended 24 h before the experiments. Male and female fish were housed separately to facilitate sex-specific selection and minimize mating behavior during preparation. One hour before the test, fish were combined in groups of 6 (3 male and 3 female) for acclimation to ensure behavioral stability. These conditions were consistently maintained across all experiments to ensure uniformity, following Organisation for Economic Co-operation and Development (OECD) guidelines.[40]

The tests were conducted based on experimental methods described in the literature.[39-41] On the day of the experiments, fish were randomly selected, placed on a moist sponge, and treated with test samples or controls via intraperitoneal (i.p.) injection with an insulin syringe (0.5 mL; UltraFine BD) with a 30-gauge needle. Before and after drug applications, the animals were locally anesthetized with an ice cube (2-4 °C) for 5 s, and immediately transferred to beakers (250 mL) containing 150 mL of aquarium water and kept at rest for 3 min for recovery observation.

The fish were euthanized by immersion in ice water (2-4 °C) for 10 min until opercular movements completely ceased. All experimental procedures were approved by the Animal Ethics Committee of the State University of Ceará (protocol number 04983945/2021) and followed the ARRIVE guidelines.

Acute toxicity 96 h

The safety and toxicity of the compounds were determined by a 96-h acute toxicity test (LD_{50}) conducted on adult zebrafish, according to OECD guidelines.[40-42] The test was performed under the environmental conditions previously described, with each group placed in a separate 10-L aquarium. The animals (n = 6 *per* group) were treated i.p. with 20 µL of each drug at doses of 4, 20, and 40 ppm; 3% DMSO as the negative control (20 µL); and DZP at 40 ppm as the positive control. An additional untreated control group was also included.

Each drug and concentration group were observed in a separate aquarium. After injection, the animals were monitored every 3 h by a human observer during the first 24 h. For the remaining days, the fish were checked twice daily, in the early morning and late afternoon. Fish were considered dead if no movement was observed, even after gentle touching of the caudal peduncle. Dead fish were immediately removed. The lethal dose for 50% of the population (LD_{50}) was determined using the Spearman-Karber method at a 95% confidence interval implemented with MATLAB software (version 9.13.0).[43,44] Tests were performed in triplicate to ensure reproducibility.

Evaluation of locomotor activity - open field test (OFT)

The open field test (OFT) evaluates the effects of drugs on motor coordination, sedation, and muscle relaxation.[40] The test was conducted under the environmental conditions previously described. The animals (n = 6 *per* group) were treated i.p. with 20 µL of each drug at doses of 4, 20, and 40 ppm; 3% DMSO as the negative control (20 µL); and DZP at 40 ppm as the positive control. An additional untreated control group was also included.

Thirty minutes after drug administration, each animal was placed in a petri dish divided into four quadrants and filled with aquarium water. The number of line crossings was manually quantified by a trained observer, blinded to the treatment conditions, using 5-min video recordings (1080 pixels, 30 frames *per* s). A line crossing was considered whenever the body center of the fish crossed a quadrant line. The number of line crossings was recorded in a spreadsheet, and the locomotor activity was compared to both the DZP-treated group and the untreated control (100% locomotor activity).

Light/dark test

The light/dark test is a standard method used to assess anxiety-related behavior, responses to environmental stimuli, or the effects of substances in zebrafish.[45] The fish were maintained under controlled conditions for 7 days before testing. The test was conducted under the environmental conditions previously described. A

glass aquarium (30 cm × 15 cm × 20 cm) was divided equally into light and dark zones and filled with 3 cm of dechlorinated water. Thirty minutes after i.p. administration of the drugs, each fish was placed in the light zone. There were no barriers between the zones, allowing the fish to move freely. The time spent in the light zone was measured manually by a blinded observer based on 5-min video recordings (1080 pixels, 30 frames *per* second), with presence defined as the head and body of the fish fully within the light zone. Data were expressed as the amount of time spent in the light zone relative to both the DZP-treated group and the untreated control (100% locomotor activity).

Evaluation of the GABAergic neuromodulation

The involvement of the GABAergic system was evaluated using the light/dark under the conditions described in the previous sub-section.[45] All zebrafish received flumazenil (FMZ) at 4 ppm (i.p.; 20 μL) and, after 15 min, were divided into groups (n = 6 fish *per* group) for each drug concentration. A negative control group received 20 μL of 3% DMSO, and an untreated group served as the baseline. Thirty minutes after treatment, each fish was placed in the light zone. The anxiolytic effect was measured with the procedure described in the light/dark section.

Molecular docking

The interaction between the $GABA_A$ receptor and CNSL constituents was analyzed using molecular docking. The two-dimensional chemical structures of the ligands (CD, CDN, and AA), were drawn using Marvin software (version 24.3.0).[46] The lowest-energy conformations were saved and optimized with 50 cycles of the steepest descent algorithm and the Merck Molecular Force Field (MMFF94) using Avogadro software.[47-50] The ligands were classified according to their degree of unsaturation: saturated ($C_{15}H_{31}$), mono-unsaturated ($C_{15}H_{29}$), di-unsaturated ($C_{15}H_{27}$), and tri-unsaturated ($C_{15}H_{25}$).

The three-dimensional structure of the $GABA_A$ receptor was sourced from the Protein Data Bank (PDB ID: 6HUP), deposited with a resolution of 2.58 Å determined by electron microscopy.[51] Polar hydrogen atoms were added, and the non-protein residues such as water molecules and co-crystallized ligands, were removed.[52]

Molecular docking of CNSL constituents (AA, CDN, CD) against the $GABA_A$ receptor (PDB ID: 6X3Z) was performed using AutoDock Vina version 1.1.2.[53-55] The receptor's BZD binding site, located at the α_1-γ_2 subunit interface, was targeted based on co-crystallized ligand DZP. The dimensions of the grid box (126 × 100 × 126 Å) were optimized to encompass the entire binding pocket and to include key residues with a 10 Å buffer around the pocket, allowing conformational flexibility. PyMOL (version 2.5) was used to calculate the volume of the binding site (ca. 500 $Å^3$), which was used to determine the box size, covering all potential ligand-receptor interactions.[56]

The center coordinates (x = 25.5, y = 10.2, z = −15.7) were set at the centroid of DZP's binding site. The exhaustiveness value was set at 8, and the top-scoring poses had a root mean square deviation (RMSD) lower than 2 Å and free binding energy (ΔG) lower than –6.0 kcal mol^{-1}.[57,58] Fifty independent simulations were conducted, resulting in 20 poses *per* simulation. The docking setup was validated by re-docking with the co-crystallized DZP, yielding a RMSD < 0.8 Å. The results were analyzed and visualized with Discovery Studio Visualizer and UCSF Chimera software.[59-61]

Statistical analysis

Behavioral data from zebrafish assays were analyzed using one-way analysis of variance (ANOVA) with multiple comparisons against a control group using Tukey's *post-hoc* test in GraphPad Prism version 7.0.[62] Comparisons were adjusted for family-wise significance at $\alpha = 0.05$, with 95% confidence intervals reported for mean differences. Data normality was assessed before ANOVA, using the Shapiro-Wilk test, and homogeneity of variances was evaluated with Levene's test, both performed in GraphPad Prism. All statistical tests used a significance level of $\alpha = 0.05$, and in the presented results, "ns" denotes non-statistical significance ($p > 0.05$).[63,64]

Results and Discussion

Silver nanoparticles characterization

The synthesis of AgAA and AgCD was confirmed by UV-Vis spectroscopy and TEM. AgAA (Figure 2a) and AgCD (Figure 2c) exhibit surface plasmon resonance extinction peaks at 423 and 414 nm, respectively, confirming the formation of silver nanoparticles. This 9-nm hypsochromic shift for AgCD indicates that smaller silver nanoparticles were formed. Absorption peaks associated with AgAA $\pi \rightarrow \pi^*$ transitions were observed at 310 nm for AA and 282 nm for AgCD. This blue shift for AgCD comes from CD's dual hydroxyl groups that act as auxochromes, which modify the electronic conjugation, altering the absorption wavelength.

AgAA (Figure 2b; TEM: 41.13 ± 19.3 nm; DLS: 167 nm; PDI: 0.342) and AgCD (Figure 2d; TEM: 40.23 ± 18.9 nm; DLS: 260 nm; PDI: 0.455) present spherical morphology in a liposomal structure formed by AA and CD, respectively. Some agglomerations were evident, hindering the accurate determination of nanoparticle sizes in certain instances. Even though most nanoparticles were encapsulated, bare nanoparticles could be observed in both cases.

Acute toxicity (96 h)

CNSL is composed of four phenolic compounds (AA, CDN, CD, and 2-MCD), which are considered protoplasmic poisons. Their amphiphilic nature facilitates the entrance into cell membranes, causing cell death and necrosis through the denaturation of proteins. Additionally, phenolic compounds can also lower the pH of the blood, leading to coagulation necrosis.[65]

The synthesis of AgNPs with natural compounds like CNSL can minimize toxicity and adverse effects by enhancing their antioxidant properties and enabling controlled release in the body.[66] CNSL constituents, AgAA and AgCD, proved to be safe, once they presented non-toxicity toward adult zebrafish during the 96 h of analysis (LC_{50} > 40 ppm). Due to insufficient mortality, precise LD_{50} estimates and 95% confidence intervals could not be calculated in MATLAB via the Trimmed Spearman-Karber macro, possibly due to compound stability or zebrafish resilience.

Evaluation of locomotor activity - open field test (OFT)

Locomotor activity is a key parameter to assess the effects of chemicals that act on the central nervous system (CNS) of zebrafish.[67] Benzodiazepines serve as positive control groups in these studies, as they are the primary treatment for anxiety, inducing sedation and, consequently, reduced locomotion.[36,52]

The analysis of line crossings during the open field test revealed a dose-dependent effect for all CNSL constituents over a 5-min analysis. Figure 3 presents the mean of line crossing ± standard error of the mean (SEM). At 40 ppm, the locomotor activity decreased for AA (52.67 ± 4.80; p = 0.0009), 56.00% ±10.61 for CD (42.50 ± 9.16; p = 0.0001), CDN (23.02 ± 2.93; p < 0.0001), and DZP (9.33 ± 0.71; p < 0.0001) when compared to untreated control group (100% locomotion; 98.5 ± 3.65).

In the OFT, AgAA induced a significant reduction at all concentrations. The most pronounced effect occurred at

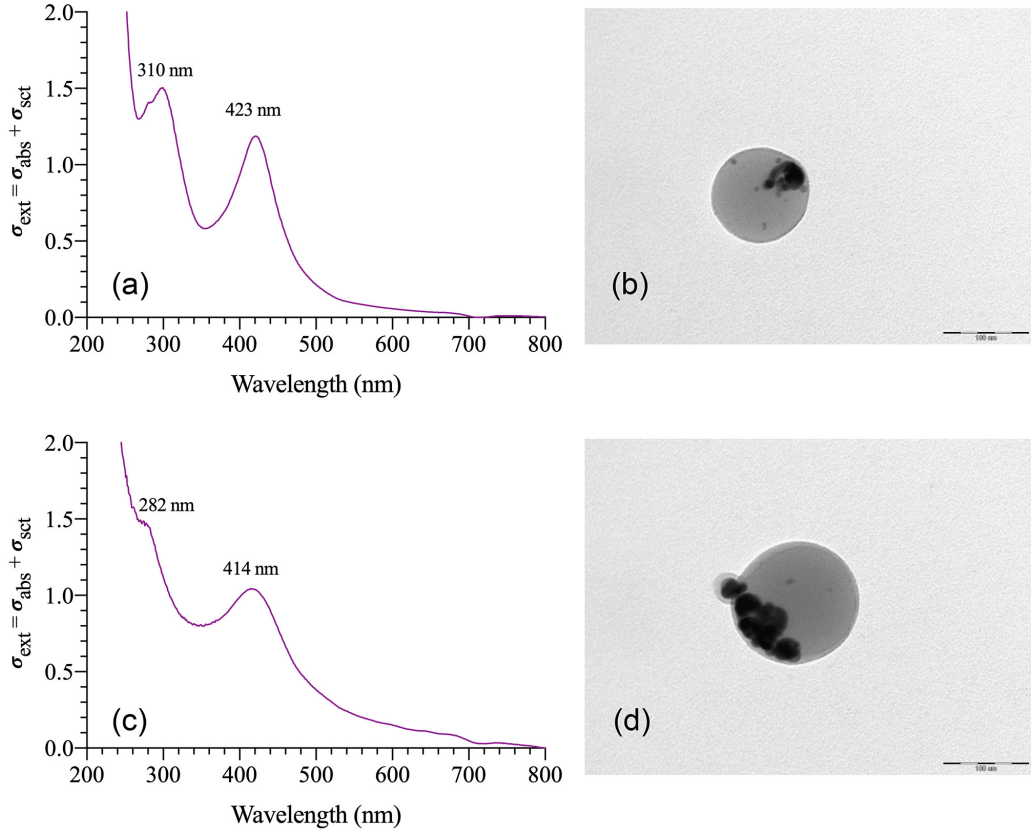

Figure 2. UV-Vis spectra of AgAA (a) and AgCD (c), and TEM micrographs of AgAA (b) and AgCD (d).

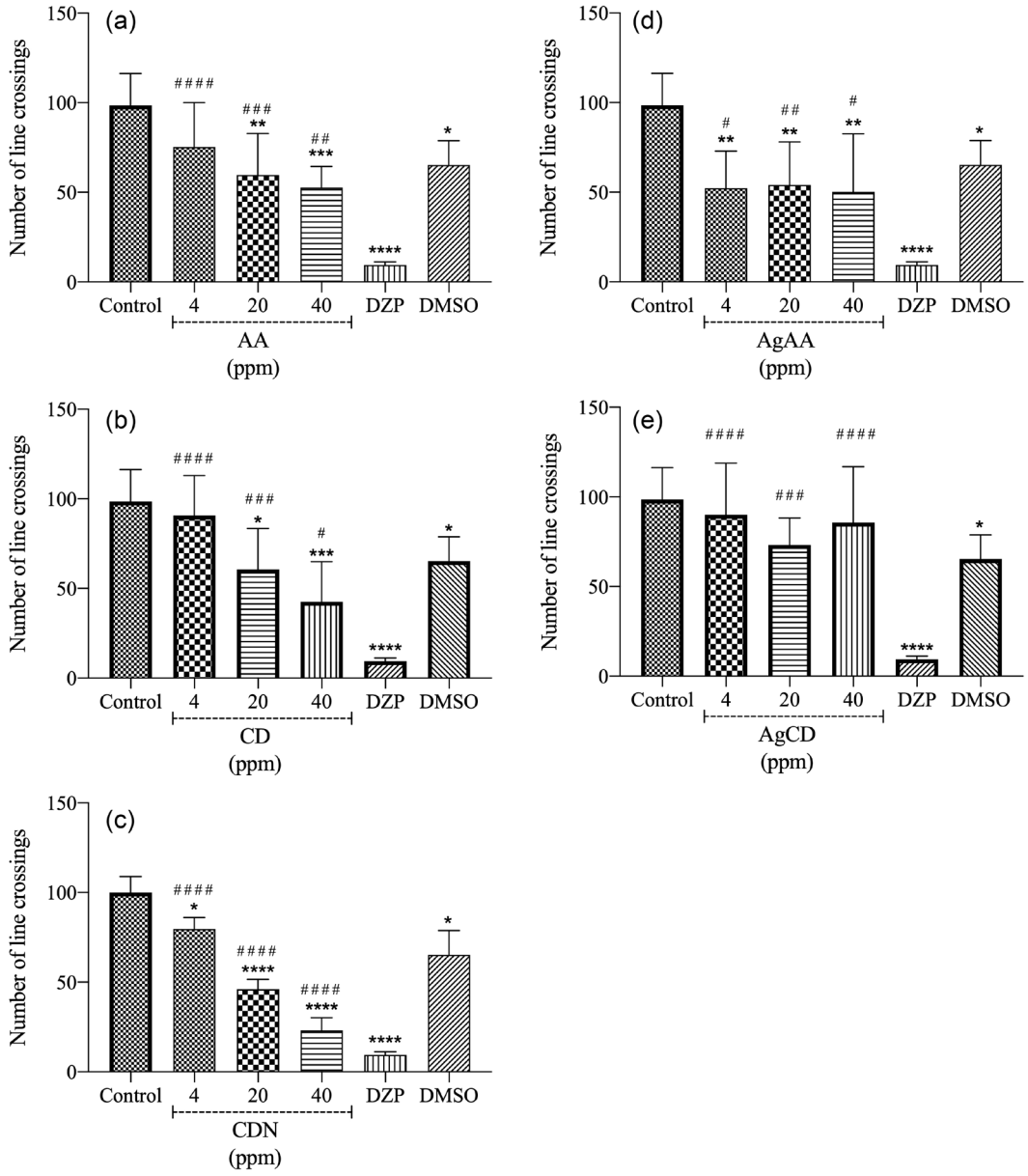

Figure 3. Effect of AA (a), CD (b), CDN (c), AgAA (d), and AgCD (e) on the locomotor behavior of zebrafish (*Danio rerio*) in the open-field test. Control: animals without treatment. DZP (40 ppm; 20 µL; i.p.). DMSO (3%; 20 µL; i.p.). The values represent the mean ± standard error of the mean for 6 animals *per* group; ANOVA followed by Tukey's multiple comparison test ($^{*}p < 0.05$, $^{**}p < 0.01$, $^{***}p < 0.001$, $^{****}p < 0.0001$ *vs.* control; $^{\#}p < 0.05$, $^{\#\#}p < 0.01$; $^{\#\#\#\#}p < 0.0001$ *vs.* DZP).

40 ppm (50.17 ± 13.24; $p = 0.0040$), indicating that AgNPs interfere with the release of AA in the cell. Contrarily, AgCD (85.67 ± 12.70; $p = 0.8843$) showed no significant impact on locomotor activity, probably due to the presence of AgNPs in the liposomal structure limiting CD release. The incorporation of AgNPs can broaden the phase transition temperature from gel to liquid-crystalline, which is a critical factor in liposome stability and drug release. Given that zebrafish are ectothermic animals, their body temperature changes with the surrounding environment, and as the water temperature was kept at 25 ± 1 °C, it may modulate the release of internal content and absorption of the liposomes, since the peak of absorption occurs near the transition temperature.[68]

Bare silver nanoparticles (AgNPs) tend to undergo oxidation, releasing Ag^{+} ions which are highly toxic, exhibit bioaccumulation potential, and pose risks to aquatic organisms and ecosystems.[69] The organic coating of AA and CD mitigates AgNPs toxicity by reducing the release of Ag^{+} ions and enhancing the nanoparticle stability. Under chronic exposure, coated AgNPs minimize long-term bioaccumulation and associated adverse effects, although extended studies are still required to fully elucidate their long-term environmental impacts.[70]

Light/dark test

Zebrafish, similar to mice, exhibit a natural avoidance of bright environments. The light-dark test exploits this behavior under the effect of some drugs (Figure 4). Anxiolytic drugs, like DZP, induce sedation and reduce this innate aversion, thereby increasing the time spent in the light zone.[71-73] CNSL derivatives contain hydroxyl groups, a structural feature common to many anxiolytic drugs, which can incorporate methoxy, methyl, dimethylamine, halogens, and nitro groups.[74,75]

Studies indicate that DZP, a $GABA_A$ receptor agonist, produces anxiolytic effects in adult zebrafish as evidenced by increased time spent in the light zone and reduced anxiety-like behaviors at 1.25-5 ppm.[13] The light/dark test confirmed the anxiolytic effect of the CNSL constituents and AgAA, as observed by the mean time of permanence in the light zone over 5 min. AA (301.33 ± 13.40 s; $p < 0.0001$), CDN (302.00 ± 12.50 s; $p < 0.0001$), CD (274.00 ± 16.97 s; $p < 0.0001$), AgAA (288.00 ± 7.63 s; $p < 0.0001$) were more efficient than DZP (244.50 ± 21.06; $p < 0.0001$) at 40 ppm.

AgCD was the only compound that exhibited significantly lower efficacy (42.17 ± 5.48 s; $p < 0.0001$)

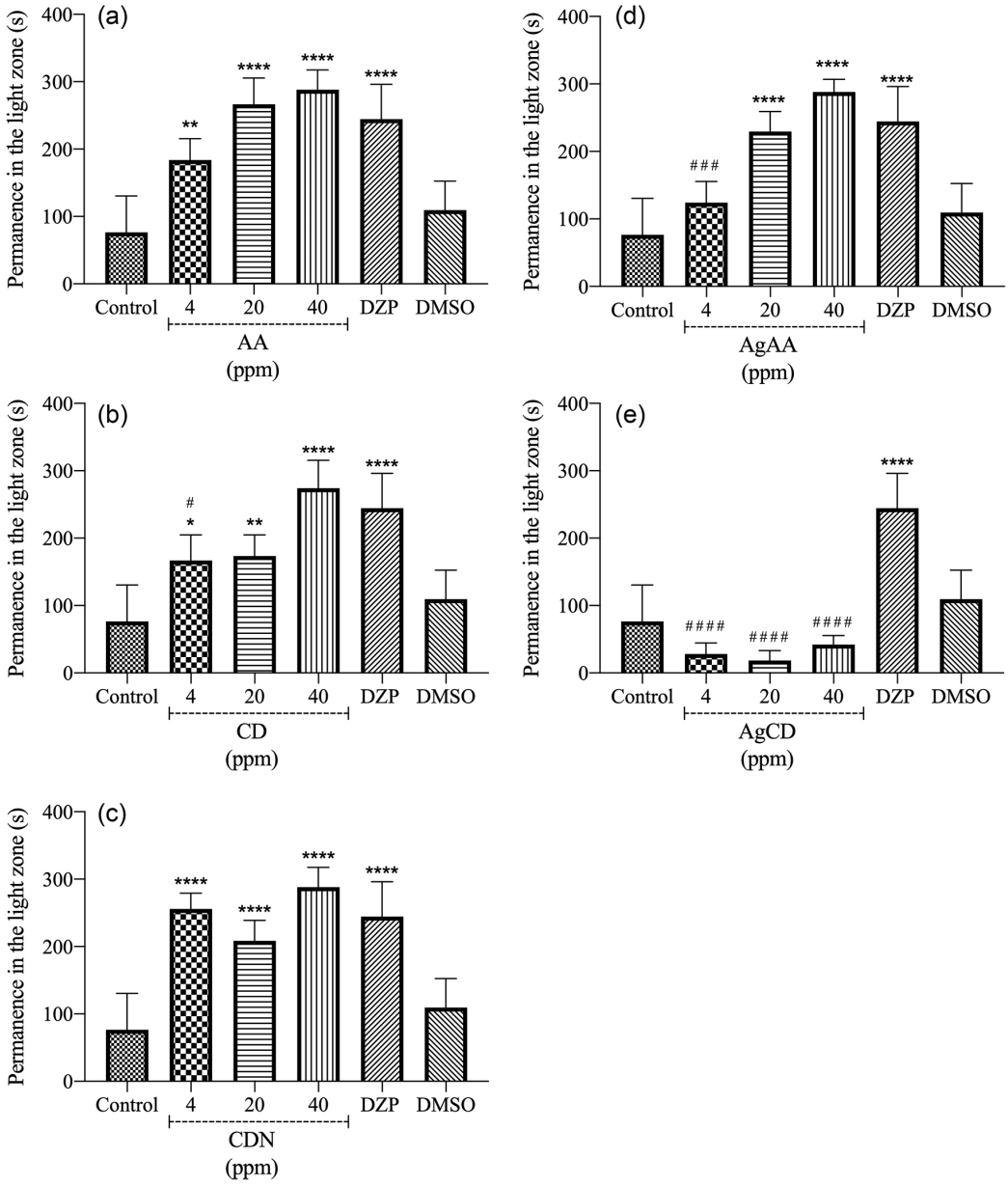

Figure 4. Effect of AA (a), CD (b), CDN (c), AgAA (d), and AgCD (e) in the light/dark test (0-5 min). Control: animals without treatment. DZP (40 ppm; 20 µL; i.p.). DMSO (3%; 20 µL; i.p.). The values represent the mean ± standard error of the mean for 6 animals *per* group; ANOVA followed by Tukey's multiple comparison test ($^{*}p < 0.05$, $^{**}p < 0.01$, $^{***}p < 0.001$, $^{****}p < 0.0001$ *vs.* control; $^{\#}p < 0.05$, $^{\#\#}p < 0.01$; $^{\#\#\#\#}p < 0.0001$ *vs.* DZP).

when compared to DZP. This outcome can be related to specific limitations in its formulation or interaction with the assay conditions, which led to its exclusion from further experimentation to prioritize more effective candidates.

The similar results from AA and AgAA indicate that the phase transition temperature of AgAA is at or below 25 ± 1 °C, while the negligible impact of AgCD indicates that the liposomal structure remains intact, hindering its absorption in this temperature range.

Involvement of the GABAergic system

To investigate the possible GABAergic-mediated anxiolytic effects of AA, CDN, CD, and AgAA, a subsequent light-dark test was carried out using FMZ (Figure 5), which is a selective competitive antagonist for the binding site of BZDs in the $GABA_A$ receptors, specifically at $\alpha_{[1–3, 5]}$, β, and γ subunits, and counteracts the sedative effects of BZD overdose.[76-78]

AgCD was excluded due to previous results in the light/dark test, while AgAA was included due to its positive behavioral results in prior experiments. FMZ attenuated the anxiolytic properties of all tested compounds, including DZP. There was a reduction in the time of permanence in the light zone (PLZ) of FMZ + CDN (73.65 ± 7.81 s; p = 0.0126), FMZ + CD (81.83 ± 8.67 s; p = 0.0052), and FMZ + AA (94.50 ± 6.03 s; p = 0.0059), similar to zebrafish treated with FMZ + DZP (38.00 ± 19.76 s; $p < 0.0001$).

The reduction of PLZ for FMZ + AgAA (73.33 ± 3.83 s; p = 0.2479) was not statistically significant, probably due to the intracellular release of silver ions (Ag^+), which can interact with FMZ polar atoms (fluorine, nitrogen, and oxygen), interfering with its effect.

Flumazenil may interact with serotonin or adenosine systems, resulting in incomplete blockade of the $GABA_A$ receptor.[4] The results show that FMZ (47.17 ± 15.20 s; p = 0.7990) did not differ statistically from the control group (76.50 ± 22.06 s), suggesting limited efficacy on its own. Nonetheless, FMZ + DZP (38.00 ± 19.76 s; $p < 0.0001$) significantly attenuated the anxiolytic effect of DZP alone (275.17 ± 15.90 s), highlighting a notable interaction that modulates the anxiolytic response.

Docking of the anxiolytic effect on the GABAergic system

Molecular docking simulations with the $GABA_A$ receptor were performed with CNSL constituents to study the anxiolytic activity. Docking reveals the structural mechanisms of ligand-receptor interactions, identifying their modes of molecular interaction with the active site of the protein ($GABA_A$).[79]

The root mean square deviation (RMSD) of atomic positions measures the average distance between the atoms of superimposed protein-ligand complexes. A RMSD < 2 Å was used to validate the docking simulations.[57] The binding affinity energy is calculated as the sum of all physical and chemical interactions modeled by the scoring function and is a fundamental parameter to assess protein-ligand complex stability. Binding affinity energy values lower than −6.0 kcal mol^{-1} were considered ideal.[58]

The simulations between the CNSL constituents with the $GABA_A$ receptor (Table 1), yielded RMSD values between 0.813 and 1.758, all within the ideal parameter.

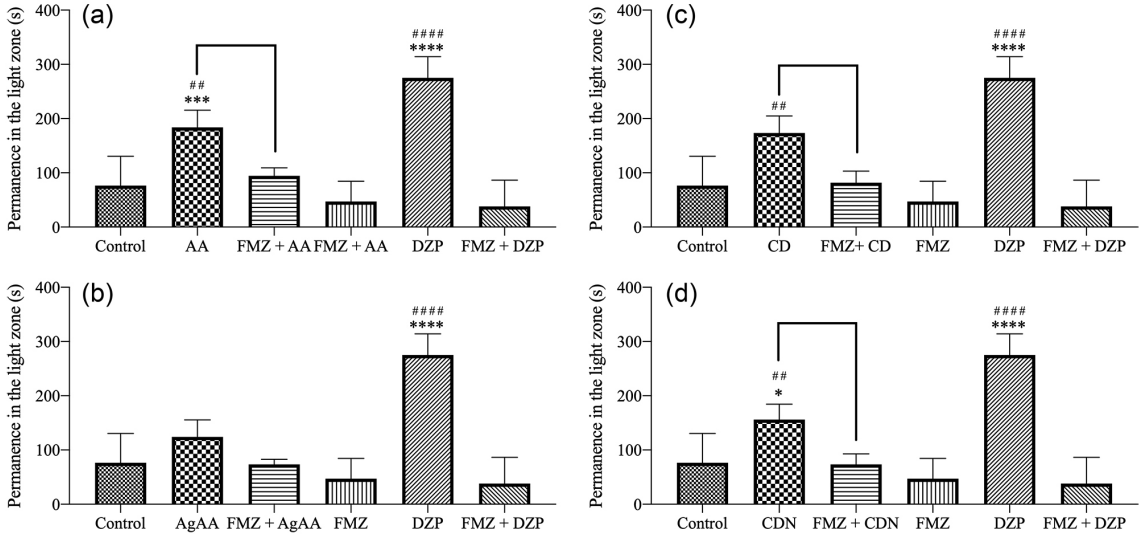

Figure 5. Effect of flumazenil on the anxiolytic effect of AA (a), AgAA (b), CD (c), and CDN (d) in the light/dark test. Control: animals without treatment. DZP (40 ppm; 20 µL; i.p.). DMSO (3%; 20 µL; i.p.). The values represent the mean ± standard error of the mean for 6 animals *per* group; ANOVA followed by Tukey's multiple comparison test ($^{*}p < 0.05$, $^{**}p < 0.01$, $^{***}p < 0.001$, $^{****}p < 0.0001$ *vs.* control; $^{\#}p < 0.05$, $^{\#\#}p < 0.01$; $^{\#\#\#\#}p < 0.0001$ *vs.* DZP).

The complexes had binding affinity energies ranging from −6.3 to −7.8 kcal mol^{-1}, except for the co-crystallized ligand DZP, which presented a binding affinity energy of −7.3 kcal mol^{-1} obtained by redocking.

The inhibition constant (K_i) is the molar concentration required to block 50% of receptor or enzyme activity.[58] K_i and pK_i values were used to refine the analysis. Lower K_i and higher pK_i values indicate higher ligand affinity to the protein; therefore, lower concentrations of the ligand are required to inhibit enzymatic activity.[80] Di-unsaturated CD, tri-unsaturated CD, tri-unsaturated CDN, and di-unsaturated AA required lower concentration to inhibit the $GABA_A$ receptor, as they presented lower K_i values compared to DZP ($K_i = 4.46 \times 10^{-6}$ mol L^{-1} and $pK_i = 5.35$), with emphasis on the di-unsaturated CD ligand ($K_i = 1.92 \times 10^{-6}$ mol L^{-1} and $pK_i = 5.72$).

The types of interaction between the ligands and amino acid residues of the $GABA_A$ receptor, along with the distances between these interactions, are detailed in Table 2 and Figure 6. In docking simulations, shorter distances between ligands (AA, CDN, and CD) and amino acid residues indicate stronger interactions with the $GABA_A$ receptor.[57,58]

The complex formed by tri-unsaturated CDN with the $GABA_A$ receptor showed interactions varying between 2.65 and 4.96 Å, including two strong hydrogen (H) bonds with serine residues (Ser205D and Ser206D) and one hydrophobic interaction with alanine (Ala79C) residue (Figure 6b).

The di-unsaturated CD complexed with the $GABA_A$ receptor presented interactions between 1.73 and 4.48 Å, including five hydrophobic interactions with tyrosine (Tyr58C, Tyr210D), alanine (Ala79C), and valine (Val203D) residues, and one strong H-bond with the Ser205D residue (Figure 6c).

The complex formed by tri-unsaturated CD with the $GABA_A$ receptor exhibited interactions ranging from 0.98 and 5.17 Å, including three hydrophobic interactions involving Tyr58C and Val203D residues, and one unfavorable donor-donor interaction with the asparagine (Asn60C) residue (Figure 6d).

The DZP complex with the $GABA_A$ receptor exhibited interactions ranging from 2.89 to 5.15 Å, including five hydrophobic interactions involving tyrosine (Tyr58C), phenylalanine (Phe77C), histidine (His102D) and valine (Val203D) residues, one π-π stacked with the Tyr210D residue and two strong H-bonds with glutamine (Gln204D) and Ser205D residues.

As seen in Figure 7, the binding energies of di-unsaturated CD (−7.8 kcal mol^{-1}, tri-unsaturated CD (−7.7 kcal mol^{-1}), tri-unsaturated CDN (−7.5 kcal mol^{-1}), and di-unsaturated AA (−7.4 kcal mol^{-1}) were lower (more energetically favorable) than DZP (−7.3 kcal mol^{-1}).

Both di- and tri-unsaturated CD present hydrophobic interactions with Tyr58C and Val203D residues; however, di-unsaturated CD forms an H-bond with Ser205D (2.88 Å compared to 2.89 Å for DZP), which enhances its affinity to the $GABA_A$ receptor. The tri-unsaturated CDN had the best performance in OFT, which may be related to H-bonds with Ser205D (2.52 Å), like DZP, and Ser206D (2.65 Å).

The di-unsaturated AA shares four stronger interactions with Tyr58C (3.94 Å), Phe77C (3.68 Å), Val203D (3.77 Å), and His102D (π-anion; 3.68 Å) residues, compared to DZP. Nonetheless, there is an unfavorable interaction with Lys156D (2.30 Å), which may limit its efficacy.

The CNSL complexes with the $GABA_A$ receptor were characterized *in silico* from energetic, structural, and chemical parameters. Their binding stability showed good correlation with the anxiolytic activity observed *in vivo* in zebrafish.

Table 1. Binding affinity, inhibition constant (K_i and pK_i), and RMSD values of the CNSL-complexes with the $GABA_A$ receptor

Ligands/Receptor	$GABA_A$			
	Energy / (kcal mol^{-1})	K_i / (mol L^{-1})	pK_i	RMSD / Å
Di-unsaturated CD	−7.8	1.92×10^{-6}	5.72	0.813
Tri-unsaturated CD	−7.7	2.27×10^{-6}	5.64	1.653
Tri-unsaturated CDN	−7.5	3.18×10^{-6}	5.49	1.404
Di-unsaturated AA	−7.4	3.77×10^{-6}	5.42	1.244
Diazepam[a]	−7.3	4.46×10^{-6}	5.35	0.719
Mono-unsaturated CD	−6.9	8.77×10^{-6}	5.05	1.942
Mono-unsaturated AA	−6.6	1.45×10^{-5}	4.84	1.956
Tri-unsaturated AA	−6.5	1.72×10^{-5}	4.76	1.932
Di-unsaturated CDN	−6.5	1.72×10^{-5}	4.76	1.892
Mono-unsaturated CDN	−6.3	2.41×10^{-5}	4.62	1.758

[a]Co-crystallized ligand (redocking). CD: cardol; CDN: cardanol; AA: anacardic acid; RMSD: root mean square deviation.

Table 2. Ligand interactions with the $GABA_A$ receptor

Ligand	Residue	Interaction	Distance / Å
Di-unsaturated CD	Tyr58C	hydrophobic	4.48
	Ala79C	hydrophobic	5.41
	Val203D	hydrophobic	4.95
	Tyr210D	hydrophobic	3.75
	Tyr210D	hydrophobic	3.88
	Ser205D	H-bond	2.88
	Tyr58C	π-π stacked	5.28
	Ser206D	unfavorable donor-donor	1.73
Tri-unsaturated CD	Tyr58C	hydrophobic	5.17
	Val203D	hydrophobic	4.52
	Val203D	hydrophobic	5.37
	Asn60C	unfavorable donor-donor	0.98
Tri-unsaturated CDN	ALA79C	hydrophobic	4.96
	Ser205D	H-bond	2.52
	Ser206D	H-bond	2.65
Di-unsaturated AA	Tyr58C	hydrophobic	3.94
	Phe77C	hydrophobic	3.68
	Val203D	hydrophobic	3.77
	Lys156D	H-bond	4.26
	His102D	π-anion	3.68
	His102D	attractive charge	4.26
	Lys156D	attractive charge	4.23
	Lys156D	unfavorable donor-donor	2.30
Diazepam[a]	Tyr58C	hydrophobic	4.62
	Phe77C	hydrophobic	5.10
	His102D	hydrophobic	4.35
	Val203D	hydrophobic	4.88
	Val203D	hydrophobic	5.15
	Ser205D	H-bond	2.89
Diazepam[a]	Gln204D	H-bond	3.35
	Tyr210D	π-π stacked	4.18
Mono-unsaturated CD	Glu189C	H-bond	2.11
	Gln204D	H-bond	2.32
	Ser206D	H-bond	2.46
	Tyr58C	π-π stacked	3.64
Mono-unsaturated AA	Val65C	hydrophobic	4.83
	Ile68C	hydrophobic	5.03
	Ala67C	H-bond	2.32
	Gln200C	H-bond	2.81
	Gln200C	H-bond	3.19
	Phe201C	π-π T-shaped	5.04
	Lys279D	salt bridge	4.09
Tri-unsaturated AA	Val65C	hydrophobic	4.91
	Ala67C	hydrophobic	5.39
	Lys279D	hydrophobic	4.39
	Ala67C	H-bond	2.34
	Gln200C	H-bond	2.38
	Gln200C	H-bond	2.78
	Phe201C	π-π T-shaped	5.04
	Lys279D	salt bridge	4.28
Di-unsaturated CDN	Trp246D	hydrophobic	4.64
	Tyr304E	hydrophobic	4.96
	Phe431E	π-π T-shaped	4.77
Mono-unsaturated CDN	Val65C	hydrophobic	4.56
	Tyr199C	H-bond	1.90
	Gln200C	H-bond	2.78
	Phe201C	π-π T-shaped	4.88
	Val65C	unfavorable donor-donor	1.38

[a]Co-crystallized ligand. CD: cardol; CDN: cardanol; AA: anacardic acid.

Molecular docking predicts ligand binding with the $GABA_A$ receptor but omits explicit water molecules, which can potentially affect H-bonds (e.g., Ser205D, Ser206D) and cause solvation effects. Additionally, rigid receptor models often neglect protein flexibility, and scoring functions may inaccurately estimate hydrophobic interactions, like Tyr58C and Val203D or π-π stacking with Tyr210D.

These limitations can be eliminated by molecular dynamics simulations, which validate binding poses by incorporating solvent effects and refine binding free energy with methods such as Molecular Mechanics Poisson-Boltzmann Surface Area (MM-PBSA).

Conclusions

In vivo test in zebrafish confirmed the anxiolytic potential of CNSL constituents (AA, CDN, and CD) and AgAA. The association of silver nanoparticles with AA formed a water-soluble liposome with a controlled-release mechanism that maintains the anxiolytic nature of AA.

In the OFT at 40 ppm, CDN reduced zebrafish's

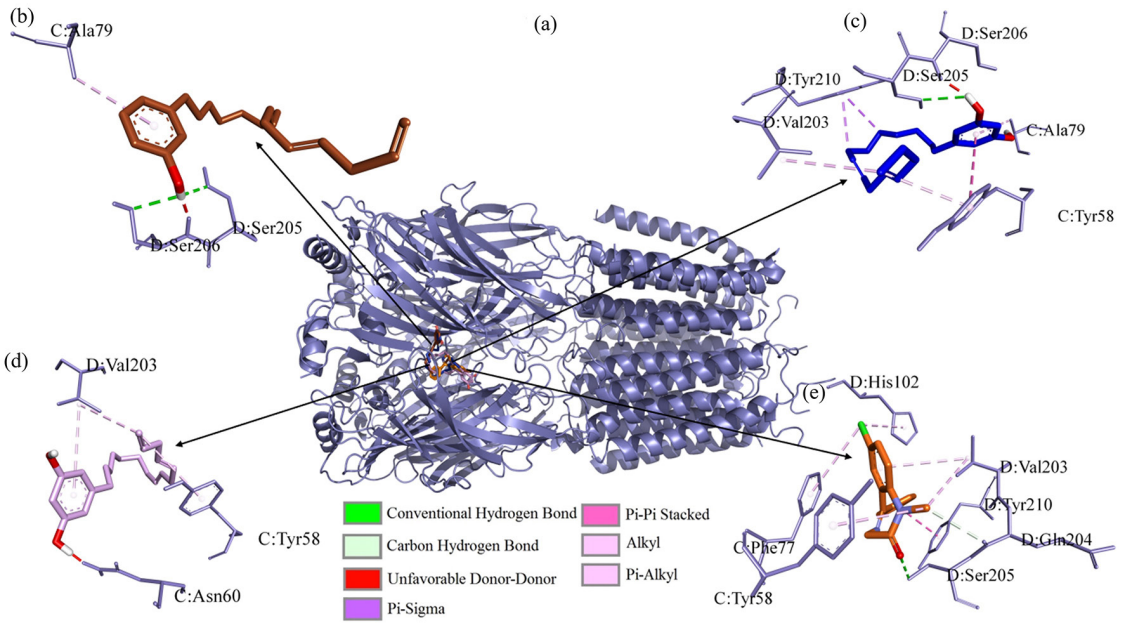

Figure 6. $GABA_A$ receptor interaction complex with ligands (a); interaction maps of the tri-unsaturated cardanol (b), di-unsaturated cardol (c), tri-unsaturated cardol (d), and the co-crystallized inhibitor diazepam (e).

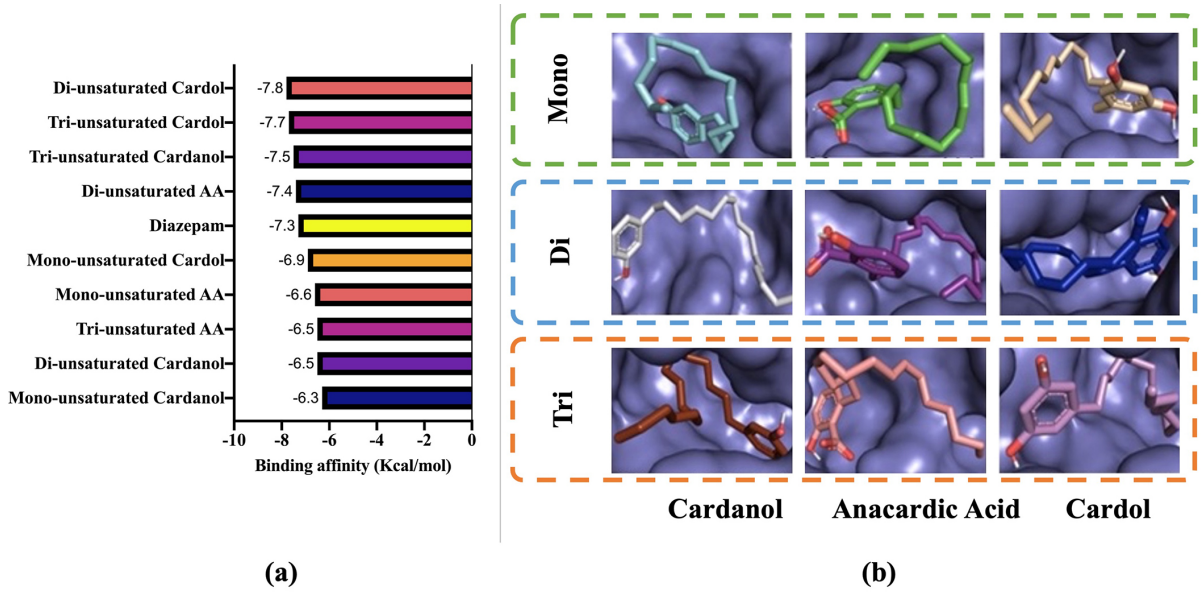

Figure 7. Results of molecular docking affinity energy (a) receptor-ligand complexes formed (b).

locomotion by 76.98%, approaching DZP. CNSL constituents and AgAA outperformed DZP in the light/dark test. AgCD was excluded due to ineffectiveness in both assays. Flumazenil reversed the anxiolytic effect of all tested drugs, confirming the involvement in the GABAergic system.

Molecular docking analysis revealed that di and tri-unsaturated CD, tri-unsaturated CDN, and di-unsaturated AA possess greater binding affinity energies (−7.4 to −7.8 kcal mol^{-1}) to the $GABA_A$ receptor than diazepam (−7.3 kcal mol^{-1}). Tri-unsaturated CDN showed the strongest hydrogen bond with Ser205D residue, thereby confirming *in vivo* efficacy.

In vivo and *in silico* studies confirmed that CNSL derivatives act as novel anxiolytic agents; however, further studies are necessary to confirm their therapeutic efficacy.

Supplementary Information

Supplementary information (Figures S1-S15) is available free of charge at http://jbcs.sbq.org.br as PDF file.

Data Availability Statement

The authors confirm that the data supporting the findings of this study are available within the article and its supplementary materials.

Acknowledgments

This study was financed in part by the Coordenação de Aperfeiçoamento de Pessoal de Nível Superior - Brasil (CAPES) - Finance Code 001. The authors also acknowledge the Conselho Nacional de Desenvolvimento Científico e Tecnológico - Brasil (CNPq) for financial support and scholarship, Amêndoas do Brasil LTDA for providing the cashew nut shell liquid (CNSL), and Centro Nordestino de Aplicação e Uso da Ressonância Magnética Nuclear (CENAUREMN) - UFC for NMR analyses.

Author Contributions

Thayllan T. Bezerra for conceptualization, formal analysis, methodology, visualization, writing original draft; Mayara O. Almeida for formal analysis, investigation, writing original draft; Pergentino N. M. Júnior for formal analysis, resources; Emerson Y. A. Sousa for investigation; Maria K. A. Ferreira for data curation, investigation, software; Antonio W. Silva for investigation; Giuseppe Mele for writing (review and editing); Emmanuel S. Marinho for methodology, software; Hélcio S. Santos for data curation, methodology, software, supervision; Jane E. S. A. Menezes for project administration, supervision; Diego Lomonaco for supervision, writing (review and editing); Selma E. Mazzetto for conceptualization, funding acquisition, project administration, resources, supervision, writing (review and editing).

References

1. World Health Organization; *Comprehensive Mental Health Action Plan 2013-2030*; World Health Organization: Geneva, Switzerland, 2021. [Link] accessed in May 2025
2. World Health Organization; *International Classification of Diseases (ICD-11)*; World Health Organization: Geneva, Switzerland, 2025. [Link] accessed in May 2025
3. Santomauro, D. F.; Herrera, A. M. M.; Shadid, J.; Zheng, P.; Ashbaugh, C.; Pigott, D. M.; Abbafati, C.; Adolph, C.; Amlag, J. O.; Aravkin, A. Y.; Bang-Jensen, B. L.; Bertolacci, G. J.; Bloom, S. S.; Castellano, R.; Castro, E.; Chakrabarti, S.; Chattopadhyay, J.; Cogen, R. M.; Collins, J. K.; Dai, X.; Dangel, W. J.; Dapper, C.; Deen, A.; Erickson, M.; Ewald, S. B.; Flaxman, A. D.; Frostad, J. J.; Fullman, N.; Giles, J. R.; Giref, A. Z.; Guo, G.; He, J.; Helak, M.; Hulland, E. N.; Idrisov, B.; Lindstrom, A.; Linebarger, E.; Lotufo, P. A.; Lozano, R.; Magistro, B.; Malta, D. C.; Månsson, J. C.; Marinho, F.; Mokdad, A. H.; Monasta, L.; Naik, P.; Nomura, S.; O'Halloran, J. K.; Ostroff, S. M.; Pasovic, M.; Penberthy, L.; Reiner Jr, R. C.; Reinke, G.; Ribeiro, A. L. P.; Sholokhov, A.; Sorensen, R. J. D.; Varavikova, E.; Vo, A. T.; Walcott, R.; Watson, S.; Wiysonge, C. S.; Zigler, B.; Hay, S. I.; Vos, T.; Murray, C. J. L.; Whiteford, H. A.; Ferrari, A. J.; *Lancet* **2021**, *398*, 1700. [Crossref]
4. da Silva, A. W.; Ferreira, M. K. A.; Rebouças, E. L.; Mendes, F. R. S.; Moura, A. L. S.; Marinho, M. M.; Menezes, J. E. S. A.; Marinho, E. S.; Santos, H. S.; Teixeira, A. M. R.; *Naunyn-Schmiedeberg's Arch. Pharmacol.* **2021**, *394*, 2023. [Crossref]
5. Wang, X.; Yang, M.; Ren, L.; Wang, Q.; Liang, S.; Li, Y.; Li, Y.; Zhan, Q.; Huang, S.; Xie, K.; Liu, J.; Li, X.; Wu, S.; *Psychiatry Res.* **2024**, *335*, 115828. [Crossref]
6. Junkes, L.; Mendlowicz, M. V.; Shader, R.; Nardi, A. E.; *Pharmacol. Res.* **2024**, *207*, 107310. [Crossref]
7. Buxeraud, J.; Faure, S.; *Actual. Pharm.* **2020**, *59*, 1. [Crossref]
8. Zhang, Y.; Shi, Y.; Tang, J.; Chen, K.; Wu, M.; Wu, X.; Qiu, X.; *Aquat. Toxicol*. **2022**, *275*, 107063. [Crossref]
9. Zahid, H.; Tsang, B.; Ahmed, H.; Lee, R. C. Y.; Tran, S.; Gerlai, R.; *Prog. Neuropsychopharmacol. Biol. Psychiatry* **2018**, *83*, 127. [Crossref]
10. Kim, J. J.; Hibbs, R. E.; *Trends Biochem. Sci.* **2021**, *46*, 502. [Crossref]
11. Chang, Y.; Xie, X.; Liu, Y.; Liu, M.; Zhang, H.; *Biomed. Pharmacother.* **2024**, *173*, 116329. [Crossref]
12. Hasin, D. S.; O'Brien, C. P.; Auriacombe, M.; Borges, G.; Bucholz, K.; Budney, A.; Compton, W. M.; Crowley, T.; Ling, W.; Petry, N. M.; Schuckit, M.; Grant, B. F.; *Am. J. Psychiatry* **2013**, *170*, 834. [Crossref]
13. Kummer, I.; Reissigová, J.; Lukačišinová, A.; Ortner Hadžiabdić, M.; Stuhec, M.; Liperoti, R.; Finne-Soveri, H.; Onder, G.; Van Hout, H.; Fialová, V.; *Ann. Med*. **2024**, *56*, 2357232. [Crossref]
14. Kaye, A. D.; Tassin, J. P.; Upshaw, W. C.; Robichaux, C. M.; Frolov, M. V.; Dupaquier, M. M.; Fox, J. E.; Sterritt, J.; Mathew, J.; Shekoohi, S.; Kaye, A. M.; Edinoff, A. N.; *Neurol. Ther.* **2024**, *13*, 965. [Crossref]
15. Cueto-Escobedo, J.; German-Ponciano, L. J.; Guillén-Ruiz, G.; Soria-Fregozo, C.; Herrera-Huerta, E. V.; *Front. Behav. Neurosci.* **2022**, *15*, 795285. [Crossref]
16. Sharma, P.; Gaur, V. K.; Sirohi, R.; Larroche, C.; Kim, S. H.; Pandey, A.; *Ind. Crops Prod.* **2020**, *152*, 112550. [Crossref]
17. Wu, H.; Li, Q.; Yu, H.; Gu, M.; Wang, Y.; Xu, C.; Liao, Z.; *Ind. Crops Prod*. **2023**, *203*, 117168. [Crossref]
18. Mazzetto, S. E.; Lomonaco, D.; Mele, G.; *Quim. Nova* **2009**, *32*, 732. [Crossref]
19. Mota, J. P. F.; Ribeiro, V. G. P.; Silva, F. L. F.; Junior, A. E. C.; Oliveira, D. R.; Kotzebue, L. R. V.; Mele, G.; Lomonaco, D.; Mazzetto, S. E.; *Sep. Sci. Technol.* **2016**, *51*, 2473. [Crossref]
20. Veeramanoharan, A.; Kim, S.; *RSC Adv*. **2024**, *14*, 25429. [Crossref]

21. Souza, N. O.; Cunha, D. A.; Rodrigues, N. S.; Pereira, A. L.; Medeiros, E. J. T.; Pinheiro, A. A.; Vasconcelos, M. A.; Neto, L. G. N.; Bezerra, T. T.; Mazzetto, S. E.; Lomonaco, D.; Teixeira, E. H.; Saboia, V. P. A.; *Arch. Oral Biol.* **2022**, *133*, 105299. [Crossref]
22. Carvalho, G. H. F.; Santos, M. L.; Monnerat, R.; Andrade, M. A.; Andrade, M. G.; Santos, A. B.; Bastos, I. M. D.; Santana, J. M.; *Chem. Biodiversity* **2019**, *16*, e1800468. [Crossref]
23. Almeida, M. O.; Bezerra, T. T.; Lima, N. M. A.; Sousa, A. F.; Trevisan, M. T. S.; Ribeiro, V. G. P.; Lomonaco, D.; Mazzetto, S. E.; *J. Braz. Chem. Soc.* **2019**, *30*, 2634. [Crossref]
24. Kanyaboon, P.; Saelee, T.; Suroengrit, A.; Hengphasatporn, K.; Rungrotmongkol, T.; Chavasiri, W.; Boonyasuppayakorn, S.; *Sci. Rep.* **2018**, *8*, 16643. [Crossref]
25. Lima, N. M. A.; Bezerra, T. T.; Almeida, M. O.; Rodrigues, N. L. C.; Braga, C. H. C.; Miranda, J. I. S.; Mazzetto, S. E.; *Photodiagn. Photodyn. Ther*. **2021**, *33*, 102083. [Crossref]
26. Gomes Jr., A. L.; Tchekalarova, J. D.; Machado, K. C.; Moura, A. K. S.; Paz, M. F. C. J.; Mata, A. M. O. F.; Nogueira, T. R.; Islam, M. T.; Rios, M. A. S.; Citó, A. M. G. L.; Uddin, S. J.; Shilpi, J. A.; Das, A. K.; Lopes, L. S.; Melo-Cavalcante, A. A. C.; *IUBMB Life* **2018**, *70*, 420. [Crossref]
27. da Silva Jr., R. R. S.; Rodrigues, V. I. O.; Carvalho, C. F. M.; Moura, M. M. B.; Feitosa, D. D. M.; Lima, E. K. F.; Andrade, A. M.; Arraes, J. F. A.; Souza, L. N.; Knackfuss, M. I.; Cavalcanti, J. R. L. P.; Fernandes, T. A. A. M.; Santos, M. A. P.; Fonseca, I. A. T.; Costa, A. V.; Cardoso, G. A.; *Antioxidants* **2025**, *14*, 441. [Crossref]
28. Yakoup, A. Y.; Kamel, A. G.; Elbermawy, Y.; Abdelsattar, A. S.; El-Shibiny, A.; *Sci. Rep.* **2024**, *14*, 364. [Crossref]
29. Lopes, L. C. S.; Brito, L. M.; Bezerra, T. T.; Gomes, K. N.; Carvalho, F. A. A.; Chaves, M. H.; Cantanhede, W.; *An. Acad. Bras. Cienc.* **2018**, *90*, 2679. [Crossref]
30. Nowicki, M.; Tran, S.; Muraleetharan, A.; Markovic, S.; Gerlai, R.; *Pharmacol. Biochem. Behav.* **2014**, *126*, 170. [Crossref]
31. Gawel, K.; Langlois, M.; Martins, T.; Ent, W.; Tiraboschi, E.; Jacmin, M.; Crawford, A. D.; Esguerra, C. V.; *Neurosci. Biobehav. Rev.* **2020**, *116*, 1. [Crossref]
32. Jha, M.; Alam, O.; Naim, M. J.; Sharma, V.; Bhatia, P.; Sheikh, A. A.; Nawaz, F.; Alam, P.; Manaithiya, A.; Kumar, V.; Nazar, S.; Siddiqui, N.; *Eur. J. Pharm. Sci.* **2020**, *153*, 105494. [Crossref]
33. Tiraboschi, E.; Martina, S.; Ent, W.; Grzyb, K.; Gawel, K.; Cordero-Maldonado, M. L.; Poovathingal, S. K.; Heintz, S.; Satheesh, S. V.; Brattespe, J.; Xu, J.; Suster, M.; Skupin, A.; Esguerra, C. V.; *Epilepsia* **2020**, *61*, 549. [Crossref]
34. de Abreu, M. S.; Giacomini, A. C.; Demin, K. A.; Galstyan, D. S.; Zabegalov, K. N.; Kolesnikova, T. O.; Kalueff, A. V.; *Pharmacol. Biochem. Behav.* **2021**, *207*, 173205. [Crossref]
35. Lomonaco, D.; Santiago, G. M. P.; Ferreira, Y. S.; Arriaga, A. M. C.; Mazzetto, S. E.; Mele, G.; Vasapollo, G.; *Green Chem.* **2009**, *11*, 31. [Crossref]
36. Ribeiro, V. G. P.; Barreto, A. C. H.; Denardin, J. C.; Mele, G.; Carbone, L.; Mazzetto, S. E.; Sousa, E. M. B.; Fechine, P. B. A.; *J. Mater. Sci.* **2013**, *48*, 7875. [Crossref]
37. Chen, K.; Wu, M.; Chen, C.; Xu, H.; Wu, X.; Qiu, X.; *Ecotoxicol. Environ. Saf.* **2021**, *208*, 111747. [Crossref]
38. Rodwell, V.; Patil, M.; Kuht, H. J.; Neuhauss, S. C. F.; Norton, W. H. J.; Thomas, M. G.; *Biology* **2024**, *13*, 4. [Crossref]
39. Magalhães, F. E. A.; de Sousa, C. A. P. B.; Santos, S. A. A. R.; Menezes, R. B.; Batista, F. L. A.; Abreu, A. O.; de Oliveira, M. V.; Moura, L. F. W. G.; Raposo, R. S.; Campos, A. R.; *Zebrafish* **2017**, *14*, 422. [Crossref]
40. Organisation for Economic Co-operation and Development (OECD); *Test No. 203: Fish, Acute Toxicity Test, OECD Guidelines for the Testing of Chemicals*, *Section 2*; OECD Publishing: Paris, France, 2019. [Link] accessed in May 2025
41. Balasubramanian, S.; Rangasamy, S.; Vivekanandam, R.; Perumal, E.; *Chemosphere* **2023**, *339*, 139681. [Crossref]
42. Amali, M. O.; Atunwa, S. A.; Aiyelero, O. M.; Omotesho, Q. A.; *IBRO Rep.* **2019**, *7*, 42. [Crossref]
43. *Matlab*, version 9.13.0; MathWorks, Natick, USA, 2022.
44. Stone, B.; *Trimmed Spearman-Karber Method*, MATLAB Central File Exchange; https://www.mathworks.com/matlabcentral/fileexchange/28479-trimmed-spearman-karber-method, accessed in May 2025.
45. Organisation for Economic Co-operation and Development; *Test No. 236: Fish Embryo Acute Toxicity (FET) Test, OECD Guidelines for the Testing of Chemicals, Section 2*; OECD Publishing: Paris, France, 2013. [Link] accessed in May 2025.
46. *Marvin*, version 24.3.0; ChemAxon, Budapest, Hungary, 2025.
47. Benneh, C. K.; Biney, R. P.; Mante, P. K.; Tandoh, A.; Adongo, D. W.; Woode, E.; *J. Ethnopharmacol.* **2017**, *207*, 129. [Crossref]
48. Hanwell, M. D.; *Avogadro*, version 1.2.0; Avogadro Chemistry Development Team, Pittsburgh, USA, 2025.
49. Halgren, T. A.; *J. Comput. Chem.* **1996**, *17*, 490. [Crossref]
50. Hanwell, M. D.; Curtis, D. E.; Lonie, D. C.; Vandermeersch, T.; Zurek, E.; Hutchison, G. R.; *J. Cheminform.* **2012**, *4*, 17. [Crossref]
51. Masiulis, S.; Desai, R.; Uchański, T.; Serna Martin, I.; Laverty, D.; Karia, D.; Malinauskas, T.; Zivanov, J.; Pardon, E.; Kotecha, A.; Steyaert, J.; Miller, K. W.; Aricescu, A. R.; *Nature* **2019**, *565*, 454. [Crossref]
52. Yan, J.; Zhang, G.; Pan, J.; Wang, Y.; *Int. J. Biol. Macromol.* **2014**, *64*, 213. [Crossref]
53. Kim, J. J.; Gharpure, A.; Teng, J.; Zhuang, Y.; Howard, R. J.; Zhu, S.; Noviello, C. M.; Walsh Jr., R. M.; Lindahl, E.; Hibbs, R. E.; *Nature* **2020**, *585*, 303. [Crossref]
54. *AutoDock Vina*, version 1.1.2; Scripps Research Institute, La Jolla, USA, 2011.
55. Trott, O.; Olson, A. J.; *J. Comput. Chem.* **2009**, *31*, 455. [Crossref]

56. *PyMOL*, version 2.5; Schrödinger LLC, New York, USA, 2021.
57. Yusuf, D.; Davis, A. M.; Kleywegt, G. J.; Schmitt, S.; *J. Chem. Inf. Model.* **2008**, *48*, 1411. [Crossref]
58. Shityakov, S.; Förster, C.; *Adv. Appl. Bioinform. Chem.* **2014**, *7*, 23. [Crossref]
59. *BIOVIA Discovery Studio Visualizer*, version 2019; Dassault Systèmes; San Diego, USA, 2019.
60. *UCSF Chimera*, version 1.19; University of California, San Francisco, USA, 2004.
61. Pettersen, E. F.; Goddard, T. D.; Huang, C. C.; Couch, G. S.; Greenblatt, D. M.; Meng, E. C.; Ferrin, T. E.; *J. Comput. Chem.* **2004**, *25*, 1605. [Crossref]
62. *GraphPad Prism*, version 7.0; GraphPad Software Inc.; San Diego, USA, 2016.
63. Hanusz, Z.; Tarasinska, J.; Zielinski, W.; *REVSTAT-Stat. J.* **2016**, *14*, 89. [Crossref]
64. Gastwirth, J. L.; Gel, Y. R.; Miao, W.; *Stat. Sci.* **2009**, *24*, 343. [Crossref]
65. Kraig, R. P.; Petito, C. K.; Plum, F.; Pulsinelli, W. A.; *J. Cereb. Blood Flow Metab.* **1987**, *7*, 379. [Crossref]
66. Abdel-Aty, A. M.; Barakat, A. Z.; Bassuiny, R. I.; Mohamed, S. A.; *Sci. Rep*. **2023**, *13*, 15605. [Crossref]
67. Gupta, P.; Khobragade, S.; Srinivasan, M. R.; Shingatgeri, V.; Rajaram, S. M.; *Drug Dev. Ther.* **2014**, *5*, 127. [Crossref]
68. De Leo, V.; Maurelli, A. M.; Giotta, L.; Catucci, L.; *Colloids Surf., B* **2022**, *218*, 112737. [Crossref]
69. Kusi, J.; Maier, K. J.; *Aquat. Toxicol.* **2022**, *242*, 106016. [Crossref]
70. Samal, D.; Khandayataray, P.; Sravani, M.; Murthy, M. K.; *Environ. Sci. Pollut. Res.* **2024**, *31*, 8400. [Crossref]
71. Gebauer, D. L.; Pagnussat, N.; Piato, A. L.; Schaefer, I. C.; Bonan, C. D.; Lara, D. R.; *Pharmacol. Biochem. Behav*. **2011**, *99*, 480. [Crossref]
72. Maximino, C.; Brito, T. M.; Dias, C. A. G. M.; Gouveia Jr., A.; Morato, S.; *Nat. Protoc.* **2010**, *5*, 209. [Crossref]
73. Stewart, A.; Gaikwad, S.; Kyzar, E.; Green, J.; Roth, A.; Kalueff, A. V.; *Neuropharmacology* **2012**, *62*, 135. [Crossref]
74. Ertl, P.; Altmann, E.; McKenna, J. M.; *J. Med. Chem.* **2020**, *63*, 8408. [Crossref]
75. Higgs, J.; Wasowski, C.; Marcos, A.; Jukic, M.; Pavan, C. H.; Gobec, S.; Pinto, F. T.; Colettis, N.; Marder, M.; *Heliyon* **2019**, *5*, e01376. [Crossref]
76. Penninga, E. I.; Graudal, N.; Ladekarl, M. B.; Jürgens, G.; *Basic Clin. Pharmacol. Toxicol.* **2016**, *118*, 37. [Crossref]
77. Bentué-Ferrer, D.; Bureau, M.; Patat, A.; Allain, H.; *CNS Drug Rev*. **1996**, *2*, 390. [Crossref]
78. Seelhammer, T. G.; DeGraff, E. M.; Behrens, T. J.; Robinson, J. C.; Selleck, K. L.; Schroeder, D. R.; Sprung, J.; Weingarten, T. N.; *Braz. J. Anesthesiol.* **2018**, *68*, 329. [Crossref]
79. Duong, T. H.; Devi, A. P.; Tran, N. M. A.; Phan, H. V. T.; Huynh, N. V.; Sichaem, J.; Tran, H. D.; Alam, M.; Nguyen, T. P.; Nguyen, H. H.; Chavasiri, W.; Nguyen, T. C.; *Bioorg. Med. Chem. Lett.* **2020**, *30*, 127359. [Crossref]
80. Kadela-Tomanek, M.; Jastrzebska, M.; Marciniec, K.; Chrobak, E.; Bebenek, E.; Boryczka, S.; *Pharmaceutics* **2021**, *13*, 781. [Crossref]

Submitted: April 13, 2025
Published online: June 18, 2025